



Biomaterial systems for evaluating the influence of ECM mechanics on anti-fibrotic therapeutic efficacy

Aryssa Simpson^{a,b,1}, Emily P. Mihalko^{a,b,1}, Caroline Fox^a, Smriti Sridharan^a, Manasi Krishnakumar^a, Ashley C. Brown^{a,b,*}

^a Joint Department of Biomedical Engineering of University of North Carolina, Chapel Hill and North Carolina State University, Raleigh, NC, 27695, USA

^b Comparative Medicine Institute, North Carolina State University, Raleigh, NC, 27606, USA

ARTICLE INFO

Keywords:

Myocardial infarction
Nanogel
Cardiac fibrosis
Tissue plasminogen activator
Y-27632
Viscoelasticity

ABSTRACT

Cardiac fibrosis is characterized by excessive accumulation and deposition of ECM proteins. Cardiac fibrosis is commonly implicated in a variety of cardiovascular diseases, including post-myocardial infarction (MI). We have previously developed a dual-delivery nanogel therapeutic to deliver tissue plasminogen activator (tPA) and Y-27632 (a ROCK inhibitor) to address MI-associated coronary artery occlusion and downregulate cell-contraction mediated fibrotic responses. Initial *in vitro* studies were conducted on glass substrates. The study presented here employs the use of polyacrylamide (PA) gels and microgel thin films to mimic healthy and fibrotic cardiac tissue mechanics. Soft and stiff polyacrylamide substrates or high and low loss tangent microgel thin films were utilized to examine the influence of cell-substrate interactions on dual-loaded nanogel therapeutic efficacy. In the presence of Y-27632 containing nanogels, a reduction of fibrotic marker expression was noted on traditional PA gels mimicking healthy and fibrotic cardiac tissue mechanics. These findings differed on more physiologically relevant microgel thin films, where early treatment with the ROCK inhibitor intensified the fibrotic related responses.

Introduction

Cardiac fibrosis results in the excessive synthesis of extracellular matrix (ECM) proteins, which impairs cardiac function. Cardiac fibrosis is implicated in numerous cardiovascular diseases, including after myocardial infarction (MI). Coronary artery disease is the number one cause of death in both the United States and Europe. Approximately 1.5 million people annually experience MI in the United States. During MI, a fibrin-rich thrombus occludes coronary arteries causing ischemic damage [1]. Subsequently, fibrosis can occur after MI during the repair and remodeling process. Following injury, cardiac fibroblasts proliferate, differentiate into myofibroblasts, and secrete additional ECM to repair the damaged tissue [2]. While critical to cardiac healing post-MI, these processes can easily become uncontrolled, resulting in stiffening of cardiac tissue and loss of cardiac function [2,3]. The mechanical properties of the ECM change during these fibrotic processes, leading to increased stiffness and decreased viscosity; these mechanical changes in

the ECM are known to further perpetuate the fibrotic process by promoting enhanced cell contractility, myofibroblastic differentiation, cell mediated activation of TGF β , and additional ECM production [3–5].

TGF β is a key mediator of fibrotic responses and has been implicated in post-MI fibrosis. [2,6,7] Previous studies have shown that TGF β activation is sensitive to mechanical changes in the ECM microenvironment; increased ECM stiffness and decreased ECM viscosity drives Rho-associated kinase (ROCK) mediated increases in cell contractility, which increases cell contractility mediated activation of the latent form of TGF β [3,8–10]. For these reasons, inhibiting the ROCK pathway is a promising strategy for mitigating fibrotic responses post-MI. However, systemic inhibition of ROCK signaling is problematic and could lead to deleterious off-target effects. Therefore, in prior studies we developed a fibrin-targeting core-shell (C/S) nanogel therapeutic to site-specifically deliver a small molecule ROCK inhibitor (Y-27632) to mitigate cardiac fibrosis post-MI. This nanogel therapeutic also contained tissue plasminogen activator (tPA) to lyse the occlusive thrombus and re-establish

* Corresponding author at: Department of Biomedical Engineering, North Carolina State University and University of North Carolina at Chapel-Hill, 1001 William Moore Dr., Raleigh, NC, 27606, USA.

E-mail address: acarso2@ncsu.edu (A.C. Brown).

¹ These authors contributed equally to this work.

<https://doi.org/10.1016/j.mbplus.2024.100150>

Received 31 January 2024; Received in revised form 29 April 2024; Accepted 18 May 2024

Available online 25 May 2024

2590-0285/© 2024 The Author(s). Published by Elsevier B.V. This is an open access article under the CC BY-NC license (<http://creativecommons.org/licenses/by-nc/4.0/>).

blood flow and attenuate any additional fibrin deposition. These C/S fibrin-specific nanogels (FSNs) were found to downregulate fibroblast α -smooth muscle actin (α -SMA) expression *in vitro* and mitigate scar tissue formation post-MI *in vivo* in a rat ischemia–reperfusion model [11]. However, more detailed understanding of cellular responses of relevant cardiac cells to dual-loaded nanogels remain to be elucidated. Additionally, our prior *in vitro* experiments were performed on glass and tissue culture plastic surfaces.

Indeed, most *in vitro* studies evaluating new anti-fibrotic therapeutics evaluate cellular responses of cells cultured on glass or tissue culture plastic, which represent stiffness values several orders of magnitude higher than those observed in healthy or fibrotic cardiac tissue. In studying cellular responses *in vitro*, fibrotic conditions can be mimicked by culturing cells on PA gels and microgel thin films that span the range of mechanics observed in healthy and fibrotic ECMs. Traditionally, to examine the relationship between ECM changes and cellular response, polyacrylamide (PA) [12] or polyethylene glycol (PEG) [13] hydrogels have been utilized. These platforms employ consistent and reproducible Young's (or elastic) Modulus. The Young's Modulus defines the ratio of stress versus strain and describes the relative stiffness of elastic materials.

To investigate the utility of drug carrying nanogels in healthy and fibrotic environments, a broad survey of relevant cardiac cell lines was performed to examine their responses on PA gels and microgel thin films. Our group has utilized microgel thin films with easily tunable viscoelastic properties to employ healthy and fibrotic mimetics with viscoelastic material properties [14]. Viscoelastic material properties refer to the ability of materials to undergo gradual deformation with a constant applied stress. Previously, our group has characterized 4-layer microgel thin films composed of different degrees of crosslinking and found an increase in intraparticle crosslinking (% bisacrylamide) led to a decrease in film loss tangent and viscosity. The microgel thin films Young's Modulus and loss tangent values for low (1 % BIS), middle (2 % BIS), and high (7 % BIS) intraparticle crosslinked films were measured to be low (1 % BIS): 95 +/- 20 kPa and 1.8 +/- 0.1; middle (2 % BIS): 107 +/- 8 kPa and 1.5 +/- 0.1, and high (7 % BIS): 114 +/- 14 kPa and 0.9 +/- 0.2, respectively. Loss tangent is defined as the ratio of loss modulus E'' to storage modulus E' . The Young's Modulus of the films are similar, while the loss tangent decreases as a function of intraparticle crosslinking, suggesting that film viscosity is decreasing with increasing particle crosslinking. Biological tissues are viscoelastic, however, controlling the viscous component of materials in a narrow range at which cells' response is challenging; especially while controlling the elastic modulus. These microgel thin films allow for fine control over material viscosity, and are therefore, an ideal material for studying how these mechanical properties of the ECM microenvironment influence cellular outcomes and efficacy of novel therapeutics. Here, we used PA gels and microgel thin films with a range of mechanical properties to evaluate the responses of cardiac cell lines to dual-loaded microgels to gain a broad understanding of the functionality of these novel therapeutics in microenvironments with mechanics spanning values observed for healthy and fibrotic tissue.

Materials and methods

Core-Shell nanogel synthesis and drug-loading

Core-shell (C/S) poly(N-isopropylacrylamide) (NIPAM) nanogels were synthesized through two sequential precipitation-polymerization reactions [11]. The initial reaction utilized 10 % BIS crosslinker to create a highly crosslinked nanogel core to facilitate optimal uptake and release of the small molecule Y-27632. After synthesis and purification of the nanogel core, a second reaction was performed to add a loosely crosslinked nanogel shell; the nanogel shell contained 2 % BIS crosslinker and 5 % Acrylic Acid (AAc). To facilitate fluorescent detection of nanogels, 0.1 % methacryloxyethyl thiocarbonyl rhodamine B

monomer (PolyScience) was added during core syntheses. Y-27632 (Fisher Scientific) and tPA (Sigma) were loaded into nanogels using a one-step swelling method, as previously published¹⁷. Prior studies demonstrated that this method results in partitioning of tPA into the loosely crosslinked shell, while Y-27632 can penetrate the highly crosslinked core. After drug loading, nanogels were purified via centrifugation then lyophilized and stored until use.

Polyacrylamide gel fabrication

Polyacrylamide (PA) gels were fabricated using a well-established method [15]. Briefly, coverslips were cleaned by sonicating in solutions of 3 % alconox, deionized water, acetone, ethanol, and isopropanol. Coverslips were dried then treated with 0.1 M NaOH, followed by APTMS, rinsing with deionized water, and treatment with 0.5 % glutaraldehyde for 30 min. PA gel solutions were then pipetted onto the treated coverslips and covered with DCDMS-treated coverslips during polymerization. Stiff PA gels were created using a solution of 2 mL acrylamide (40 %), 5.8298 mL bis-acrylamide (2 %), and 2.1702 mL deionized water polymerized with 100 μ L ammonium persulfate (APS) (10 % w/v) and 10 μ L tetramethylethylenediamine (TEMED). Soft PA gels were created using a solution of 2 mL acrylamide (40 %), 0.6998 mL bis-acrylamide (2 %), and 7.3002 mL deionized water polymerized with 100 μ L APS (10 % w/v) and 10 μ L TEMED. Following polymerization, PA gels were rinsed with deionized water and incubated in 0.2 mg/mL sulfo-SANPAH under UV light for 8 min; this treatment was performed twice. Next, two washes with 50 mM HEPES, pH 8.5 were performed and then gels were incubated with 40 μ g/mL rat tail collagen type I (Enzo Life Sciences) in HEPES buffer overnight at 4 °C. Prior to cell culture, gels were washed twice with sterile PBS then UV sterilized for 30 min. Young's modulus characterization of PA gels was conducted via atomic force microscopy (AFM) using a 16 x 16 μ m area in Contact Mode Topography. Single-force measurements were captured using cantilever tips (CP-qp-CONT-PS-A-5) with a spring constant of 30 kHz and diameter of 1.98 μ m. Duplicate measurements were performed for each sample and the Young's modulus was determined by fitting the data using the Hertz model. The Young's modulus +/- standard error of the mean of soft PA gel substrates was 20.4 \pm 0.52 and stiff PA gel substrates was 106.2 \pm 4.85 kPa (Supplementary Figure 1). This data was analyzed via a nonparametric Mann-Whitney test, displaying a p value < 0.0001.

Single microgel synthesis

Single microgels used for film fabrication were synthesized via a precipitation-polymerization reaction [14] using a total monomer concentration of 140 mM. The reaction contained 1 %, 2 %, or 7 % N,N'-methylenebis(acrylamide) (BIS), 5 % Acrylic Acid (AAc), 94 %, 93 %, or 88 % Poly(N-isopropylacrylamide)(poly-NIPam), and 0.75 and 0.3 mM sodium dodecyl sulfate (SDS), respectively. A reaction volume of 100 mL was used. Poly-NIPam, BIS, and SDS were mixed in ultrapure water, filtered using a 0.22 μ m Steriflip-GP Polyethersulfone (PES) filter, and added to a three-necked reaction vessel. Following a 1-hour equilibration at 70 °C, 5 % AAc and 1 mM ammonium persulfate (APS) were added to the reaction. The solution was stirred at 450 RPM for 5.5 h. Subsequently, the solution was filtered with glass wool to remove large aggregates then dialysis into deionized, ultrapure water with 1000 kDa dialysis tubing was used for further purification. Dialysis proceeded for 72 h with three buffer exchanges. Samples were then collected, lyophilized, and stored until further use.

Construction of viscoelastic Four-Layer film

Four-layer microgel thin films were created using centrifugal deposition. Glass coverslips were functionalized using a 1 % solution of (3-Aminopropyl) trimethoxysilane (APTMS) in 200 Proof Ethanol, for 2 h shaking at 50 RPM. Following functionalization, glass coverslips were

washed once with DI water and transferred to a new 12-well plate. Next, a 0.1 mg/mL of 1 %, 2 % or 7 % BIS microgel solution was added to the functionalized coverslips and centrifuged at 3000g for 10 min. Following centrifugation, the microgel solution was removed, coverslips washed once with DI water and a 0.05 monomolar polyethyleneimine (PEI) solution was added. The coverslips were placed on a shaker for 30 min at 50 RPM. The PEI solution was then removed, and the coverslips washed again with DI water. This process was repeated until 4 microgel layers were constructed, with the final layer being microgel particles. 4-layer thin films were sterilized for 30 min in 30 % Ethanol solution, and then incubated overnight in PBS at 4 °C. The microgel thin films Young's Modulus and Loss Tangent values for low, middle, and high intraparticle crosslinked films were 1 %: 95 +/- 20 kPa and 1.8 +/- 0.1, 2 %: 107 +/- 8 kPa and 1.5 +/- 0.1, and 7 %: 114 +/- 14 kPa and 0.9 +/- 0.2, respectively [14].

Cell culture

Neonatal rat cardiac fibroblasts (NRCF) (obtained as previously described [16]), human umbilical vein endothelial cells (HUVEC), and human aortic smooth muscle cells (HASMC) (ATCC) were evaluated in these studies. NRCF and HASMC were seeded onto PA gels or microgel thin films in a 12 well plate at 12,000 cells per well. HUVEC were seeded onto PA gels and microgel thin films in a 12 well plate at 200,000 and 100,000 cells per well, respectively. NRCFs and HASMCs were cultured in Dulbecco's Modified Eagle's Medium (DMEM) (Caisson Labs) with 2 mM L-glutamine, 1 % penicillin-streptomycin, and 10 % or 20 % fetal bovine serum (FBS, Genesee Scientific), respectively. HUVECs were cultured in endothelial cell growth media (Sigma Aldrich 211-500) with 10 % FBS, 2 mM L-glutamine, and 1 % penicillin-streptomycin.

Cells were cultured overnight, 24 h, or 48 h then washed twice with sterile PBS, fixed in 4 % paraformaldehyde (PFA) on PA gels or 95 % Methanol and 5 % Glacial Acetic Acid on microgel thin films, and then washed three times with PBS prior to immunofluorescent staining. A minimum of 4 wells per condition were analyzed, conducted in two duplicate sets of experiments for each cell type. Nanogel treatments (unloaded nanogels, tPA-loaded C/S nanogels, Y-27632-loaded C/S nanogels, or tPA and Y-27632C/S nanogels) were added to cells at a concentration of 1 mg/mL.

Fibrotic marker expression and morphology Quantification

Expression of fibrotic markers α SMA and connective tissue growth factor (CTGF) were analyzed for NRCF and HASMCs via immunofluorescent staining. Fixed cells were permeabilized with 0.1 % Triton-X 100, blocked with 1 % BSA in PBS with 0.1 % tween (PBST), and incubated with anti-actin, α SMA, clone 1A4 1:200 dilution (Sigma-Aldrich) and anti-CTGF antibody ab6992 1:200 dilution (Abcam) in 1-2 % BSA in PBST for 2 h at room temperature. Cells were treated with AlexaFluor 488 goat anti-mouse (Invitrogen) or AlexaFluor 594 goat anti-rabbit (Invitrogen) and a NucBlue Live stain (Invitrogen) in 1 % BSA in PBST for 1 h at room temperature. The protocol was consistent on microgel thin films but omitted treatment with 0.1 % Triton-X 100. Actin and VE Cadherin were measured via immunofluorescent staining for HUVECs. Following fixation, HUVECs were incubated with 2 % BSA in PBS followed by an overnight treatment at 4 °C with 1x AlexaFluor 488 Phalloidin (Thermo Fisher Scientific) and 1:100 CD144 (VE Cadherin 14-1449-82 Thermo Fisher Scientific) in 0.1 % BSA in PBS. Samples were then treated with AlexaFluor 594 goat anti-mouse (Invitrogen) in 0.1 % BSA in PBS at 4 °C overnight, followed by NucBlue Live stain. Samples were mounted in Fluoromount-G mounting medium and imaged with an ECHO labs Revolve Fluorescence Microscope (PA Gel samples), and EVOS FL Auto (microgel thin film samples). Image J was used to quantify morphological parameters, including circularity. The parameter for perfect cell circularity is 1.0. Circularity was defined as $\text{circularity} = 4\pi(\text{area}/\text{perimeter}^2)$, with lower values indicating more

polygon shaped cells, which are associated with fibrotic phenotypes. Quantification of α SMA, CTGF, actin (phalloidin), and VE Cadherin was conducted by measuring corrected total cell fluorescence using the following equation: $\text{integrated density of cell} - (\text{cell area} \times \text{mean gray value of background})$. At least 10 cells per well were analyzed per condition.

Analysis of cell viability and nanogel endocytosis

To analyze cell viability, cells were seeded on soft and stiff PA gels coated in collagen. Following a 48-hour incubation, cells were treated with 1 mg/mL of tPA and Y-27632 nanogels. After an additional 24 h incubation, cells were stained with NucBlue Live and NucGreen Dead ReadyProbes™ then imaged using an ECHO labs Revolve Fluorescence Microscope. To evaluate potential nanogel endocytosis, cells were cultured on soft or stiff PA gels. 7 h after plating cells were treated with PBS or 1 mg/mL of nanogel groups, which included rhodamine B C/S nanogels, or rhodamine B C/S nanogels conjugated to fibrin-targeting element (fibrin fragment E antibody, Affinity Biologicals). After a 24-hour incubation, cells were fixed in 4 % PFA, stained with 488 phalloidin and imaged with a Zeiss Laser Scanning Microscopy (LSM 710, Zeiss Inc., White Plains, NY). A minimum of 4 samples were analyzed per treatment group.

Evaluation of endogenous fibrinolysis

C/S nanogels were loaded with 0.029 mg/mL tPA, tPA and 0.414 mM Y-27632, 0.029 mg/mL or 0.120 mg/mL plasmin, plasmin and Y-27632 via the rehydration method described above. An absorbance-based endogenous fibrinolysis assay was then performed to measure *in vitro* clot degradation in the absence or presence of drug-loaded nanogels [17]. 1 mg/mL fibrinogen, 10.8 μ g/mL plasminogen, 1 or 3 mg/mL drug loaded nanogels, and 2.5 U/mL thrombin were combined in 25 mM HEPES, 150 mM NaCl, 5 mM CaCl₂ buffer and then dynamics of clot polymerization/degradation were determined by measuring absorbance at 350 nm every 30 s for 2 h. Negative controls included fibrinogen without thrombin and positive controls included fibrinogen without nanogels. Experiments were performed in triplicate.

Statistical analysis

Statistical analysis was performed by using GraphPad Prism 8 (GraphPad, San Diego, CA). Outlier tests were performed on all data sets prior to statistical analysis. Data was analyzed via a one-way analysis of variance with a Tukey's post-hoc test using a 95 % confidence interval. All data are presented as average \pm standard deviation.

Results

Emergent fibrotic phenotype in the absence of nanogel treatment

Fibrotic marker expression and morphological differences were first evaluated in the absence of nanogel therapeutics on PA gels and microgel thin films at various time points. Neonatal rat cardiac fibroblasts (NRCF) on stiff PA gels and low loss tangent films, compared to healthy cardiac mimetics, showed significant increases in expression of representative fibrotic markers alpha smooth muscle actin (α SMA) and connective tissue growth factor (CTGF) at all time points (t = overnight (O/N), 24-hours, and 48-hours) on stiffer PA gels (p < 0.0001) and 24-hours on low loss tangent films. Expression of α SMA and CTGF on stiff compared to soft PA gels was increased after 48 h (53,313 +/- 39,487 to 623,893 +/- 500,212 and 32,509 +/- 19,261 to 276,104 +/- 166,535, respectively) (Fig. 1). For analysis on microgel thin film cardiac mimetics, expression of α SMA at 24-hours increased with decreasing loss tangent (High (1 % BIS): 374,085 +/- 183,875, Medium (2 % BIS): 472,758 +/- 264,525, Low (7 % BIS): 517,384 +/- 212,574) (Fig. 2).

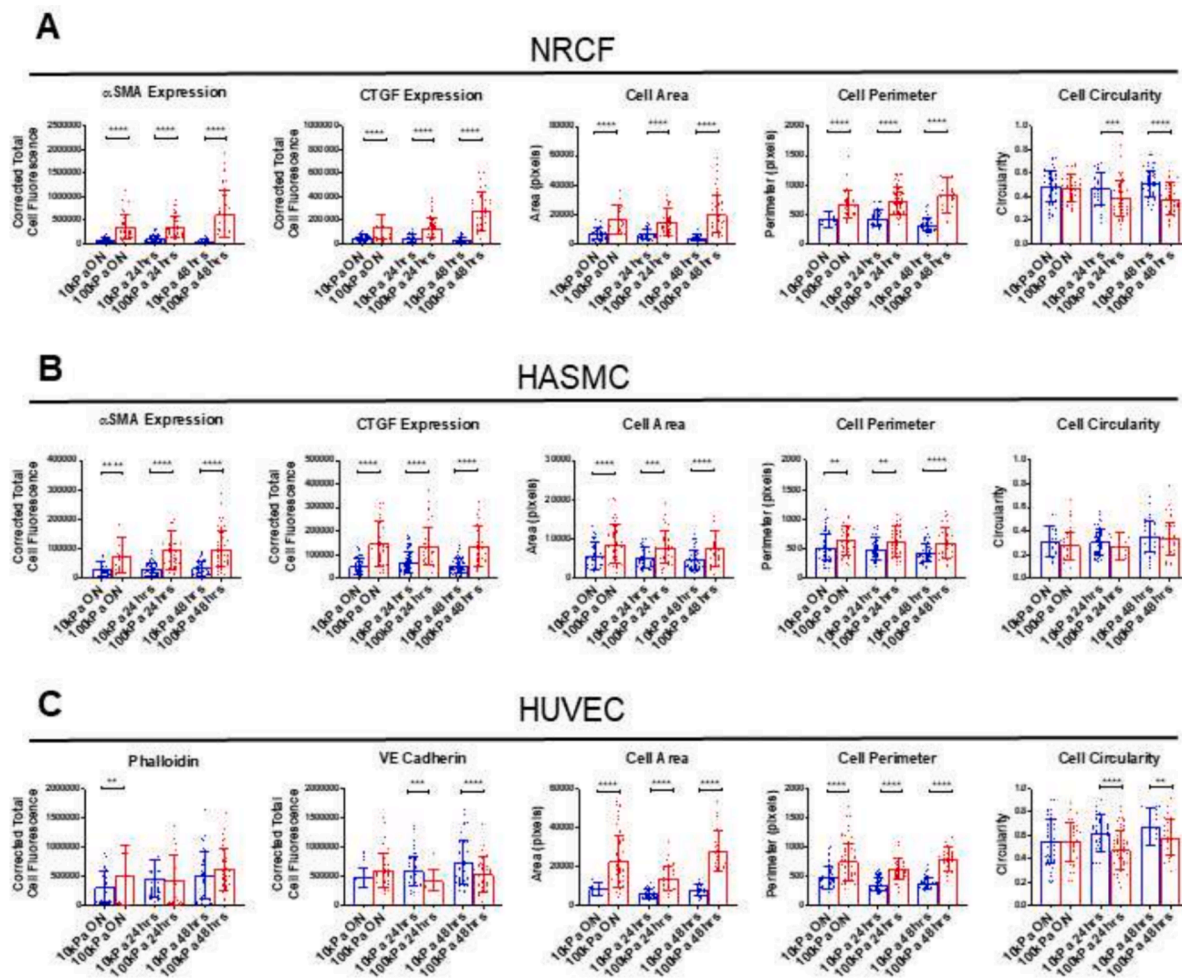


Fig. 1. Time course experiments on PA gels for cell types. (A-C) Quantification of immunofluorescent staining and morphological measurements evaluating neonatal rat cardiac fibroblasts (NRCF), human aortic smooth muscle cells (HASMC), and human umbilical vein endothelial cells (HUVEC) on soft and stiff PA gels following overnight, 24-, or 48-hours culture. A one-way analysis of variance was conducted with a Tukey's post-hoc test using a 95 % confidence interval. Mean \pm standard deviation is shown. ** $p < 0.01$, *** $p < 0.001$, **** $p < 0.0001$.

Similarly, CTGF on high loss tangent films, compared to low loss tangent films, at 24-hours was increased by factor of ~ 1.5 .

Similarly, human aortic smooth muscle cells (HASMCs) cultured on stiff PA gels showed significant increases in expression of α SMA and CTGF at all time points compared to cells cultured on soft PA gels. Specifically analyzing the fibrotic marker expression of α SMA and CTGF, following a 48 h incubation a respective 2.9 and 2.6 factor increase was noted (33,902 \pm 24,743 to 98,729 \pm 60,005 and 52,606 \pm 31,288 to 134,501 \pm 85,998 respectively). However, for HASMCs, the expression of α SMA decreased with increasing loss tangent at 24-hours (High (1 % BIS): 316,600 \pm 220,847, Medium (2 % BIS): 130,122 \pm 142,797, Low (7 % BIS): 139,605 \pm 96,146) (Fig. 2). Similarly, CTGF on high loss tangent films, compared to low loss tangent films, at 24hrs was decreased by factor of ~ 0.64 . No significant cellular morphological changes were noted in cell circularity of HASMCs at all time points. At timepoints overnight, 24-hours, and 48-hours, an increase was observed in cell area and perimeter on stiff compared to soft PA gels (Fig. 1). On microgel thin films, a slight difference was noticed in cell area and perimeter following incubation on high loss tangent at $t = 0/N$, 24-hours, and 48-hours in comparison to medium and low loss tangent substrates. Additionally, no statistical differences were noted between samples at overnight and 48-hours. Interestingly, in the absence of loaded nanogels, differences are noted in the expression of α SMA and CTGF on PA gels and microgel thin films. The comparison of different substrates allows for *in vitro* examination in the influence of

viscoelasticity on markers of cardiac fibrosis.

Human umbilical vein endothelial (HUVEC) cellular responses were also evaluated on PA gels and microgel thin films. On PA gels, minimal differences were observed in HUVEC actin expression at 24 and 48-hours. However, a significant decrease in vascular endothelial (VE)-cadherin expression was noted for HUVECs cultured on stiff PA gels compared to soft PA gels, with fluorescence values of 745,090 \pm 376,036 decreasing to 531,246 \pm 301,232. On microgel thin films, the largest differences in HUVEC actin and VE Cadherin expression were noted after 24-hours. There was a significant decrease in actin expression on medium and low loss tangent films, compared to high loss tangent substrates, with a corrected total cell fluorescence value of 351,145 \pm 415,807 decreasing to 199,917 \pm 275,977 ($\sim 54\%$) and 54,095 \pm 25,455 ($\sim 147\%$). Of note, VE Cadherin immunofluorescent staining was conducted without cell permeabilization. Decreases in VE Cadherin shown here mirror the response of impaired vascular integrity [18,19]. Examining cell morphology changes on PA gels, a significant increase in HUVEC cell area and cell perimeter was observed at all time points, and a significant reduction in cell circularity was observed after 24 and 48-hours on stiff PA gels compared to soft gels (Fig. 1), similar to previous studies [20]. The largest differences in cell area and perimeters was observed at 24hrs on microgel thin films. These data suggest a strong trend that fibroblasts, smooth muscle cells, and endothelial cells cultured using these traditional *in vitro* models mirror known responses in fibrosis.

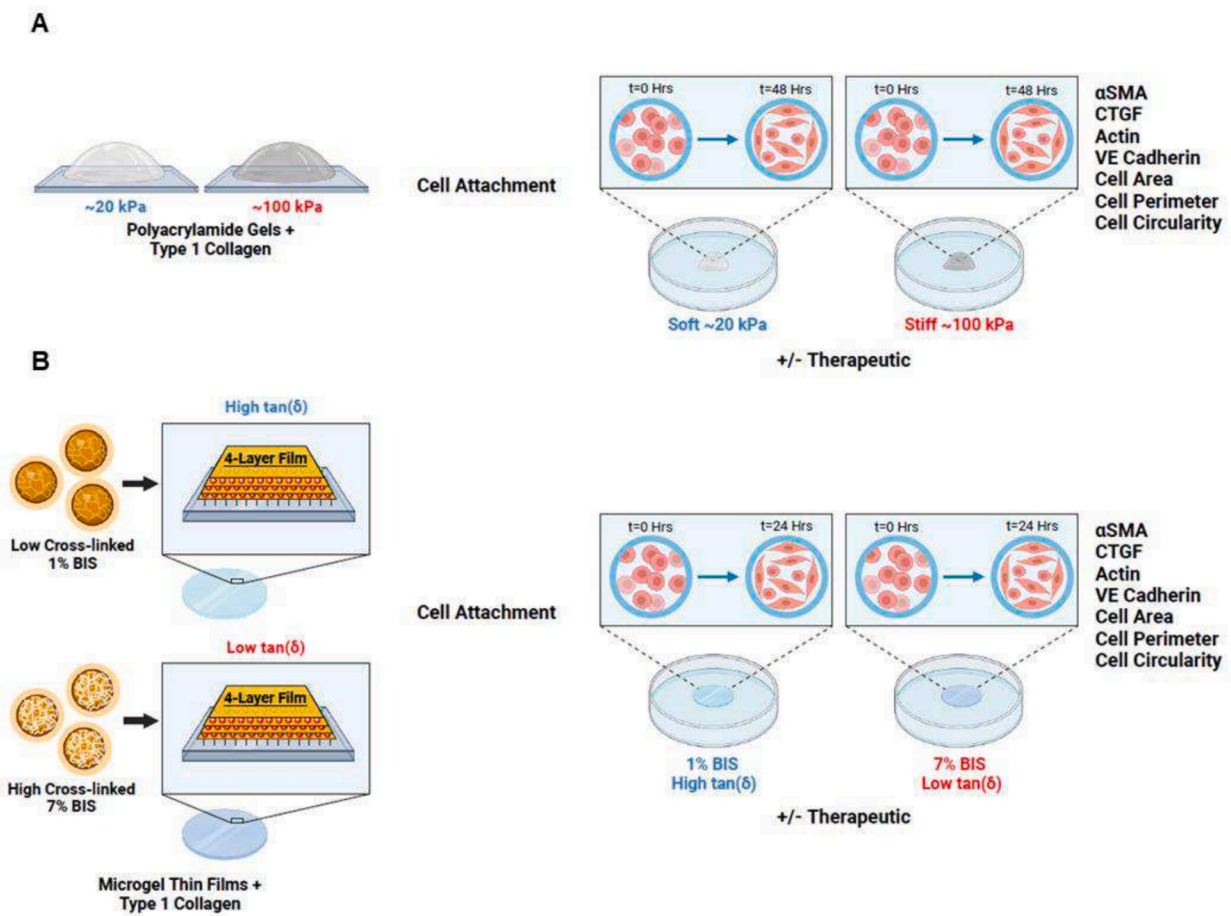


Fig. 3. Design overview for therapeutic experiments performed on PA gels and microgel thin films. A) An overview of the experimental schematic for the therapeutic experiments performed on soft (~20 kPa) and stiff (~100 kPa) PA gels. B) An overview of the experimental schematic for the therapeutic experiments performed on high loss tangent (1 % BIS) and low loss tangent (7 % BIS) microgel thin films.

Smooth muscle cell response to antifibrotic therapeutics

In the presence of drug-loaded nanogels, on both soft and stiff PA gels, a significant reduction in HASMC α SMA and CTGF expression was observed. α SMA fluorescence was reduced by 63 %, from 48,506 \pm 29,798 in controls to 25,158 \pm 17,250 in cells treated with dual-loaded nanogels on soft PA gels. Further, a reduction of 134 % from 104,239 \pm 77,472 in control samples to 20,583 \pm 17,508 in samples treated with dual-loaded nanogels on stiff PA gels. Expression of CTGF was reduced by 94 %, from 66,291 \pm 41,056 in controls to 23,961 \pm 16,559 in samples treated with dual-loaded nanogels on soft PA gels. Additional observations were noted on stiff PA gels, with a reduction by 105 % from 100,580 \pm 67,562 in control samples to 31,223 \pm 20,034 in cells treated with dual-loaded nanogel. In the presence of drug-loaded nanogels on high and low loss tangent microgel thin films, a slight increase in HASMC α SMA and CTGF expression was observed. Measuring α SMA expression, on high loss tangent films, corrected total cell fluorescence increased from 123,530 \pm 92,252 in controls to 149,403 \pm 106,755 in dual-loaded nanogel conditions (19 %). Similarly, on low loss tangent films, cell fluorescence increased from 97,384 \pm 76,222 in controls to 141,907 \pm 105,410 in dual-loaded nanogel conditions (37 %). With morphology measurements, no significant differences in HASMC cell perimeter were observed on soft PA gels, significant decreases in cell perimeter were observed on stiff PA gels with tPA and Y-27632 nanogels compared to controls. Reductions in HASMC cell circularity were also observed on both soft and stiff PA gels upon treatment with Y-27632 containing nanogels. On soft PA gels, decreased cell circularity was observed with Y-27632 nanogels with or without

dual-delivery of tPA, but on stiff PA gels, decreased cell circularity was more apparent with tPA and Y-27632 nanogels (Fig. 6). On high loss tangent films, a significant increase was detected in cell area and perimeter between controls compared to single or dual-loaded Y-27632 nanogels. Similarly, a significant decrease in cell circularity was noted. On low loss tangent films, analyzing cell area and perimeter, there was a significant increase between controls compared to single and dual-loaded Y-27632 nanogels. Similar to responses on high loss tangent films, a significant decrease in cell circularity was noted on single and dual-loaded Y-27632 nanogels (Fig. 7).

HUVEC response to antifibrotic therapeutic

HUVEC responses to antifibrotic drug-loaded nanogels were less apparent on soft compared to stiff PA gels. However, on soft PA gels there were some changes in cell morphology, including cell area, cell perimeter, and cell circularity when cultured with Y-27632-loaded nanogels compared to controls and/or tPA-loaded nanogels. On stiff PA gels, a significant increase in VE Cadherin expression was observed with Y-27632 nanogels with or without dual-delivery of tPA compared to controls, unloaded nanogels, and tPA-loaded nanogels ($p < 0.0001$) (Fig. 8). Interestingly, on microgel thin films, HUVECs responded positively to antifibrotic drug-loaded nanogels on both high and low loss tangent films. On high loss tangent films, there was a significant decrease in Actin expression and no change in VE Cadherin for controls compared to single and dual-loaded Y-27632 nanogels. On low loss tangent films, there was no change in Actin expression and a significant decrease in VE Cadherin expression on single-loaded Y-27632 nanogels

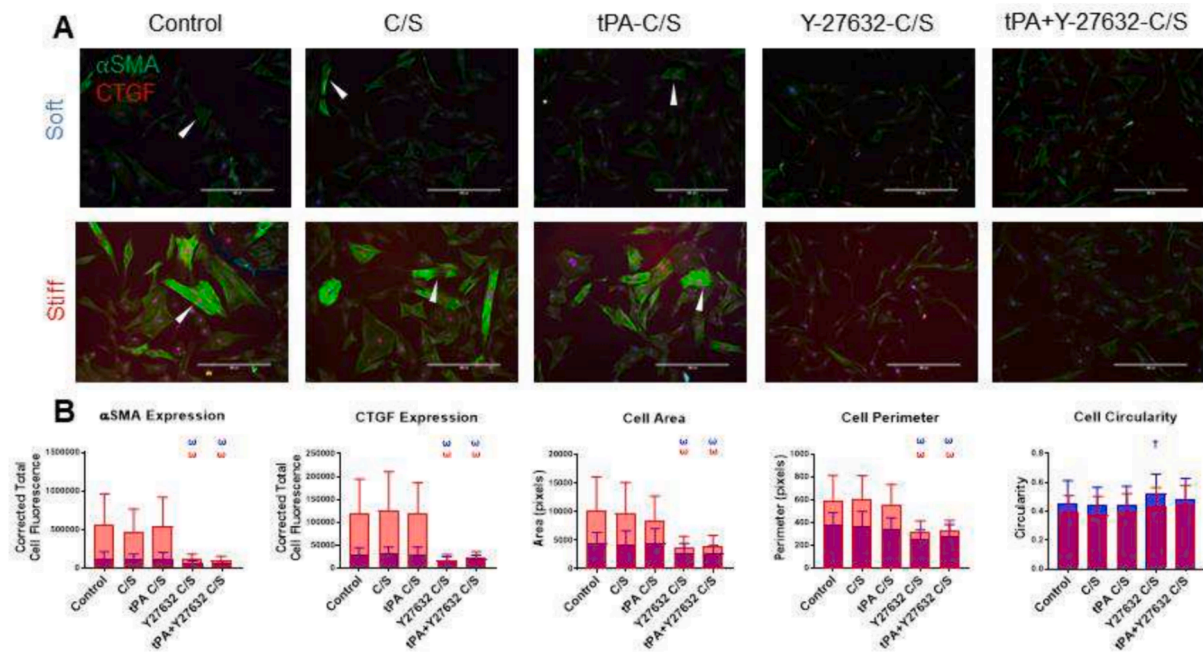


Fig. 4. Evaluation of neonatal rat cardiac fibroblasts comparing fibrotic markers and cell morphology on soft and stiff PA gels with drug-loaded nanogels. (A) Representative images of NRCF on soft and stiff PA gels. (B) Quantification of NRCF fibrotic markers on soft (blue) and stiff (red) PA gels with drug-loaded nanogel samples after 48 h. α SMA, CTGF, cell area, cell perimeter, and cell circularity measurements are shown. Stress fiber positive cells are indicated by white arrowheads. A one-way analysis of variance was conducted with a Tukey's post-hoc test using a 95 % confidence interval. Mean \pm standard deviation is shown. $\dagger p < 0.05$, $\ddagger p < 0.01$, $\Omega p < 0.001$, $\omega p < 0.0001$. Scale bar = 400 μ m. (For interpretation of the references to colour in this figure legend, the reader is referred to the web version of this article.)

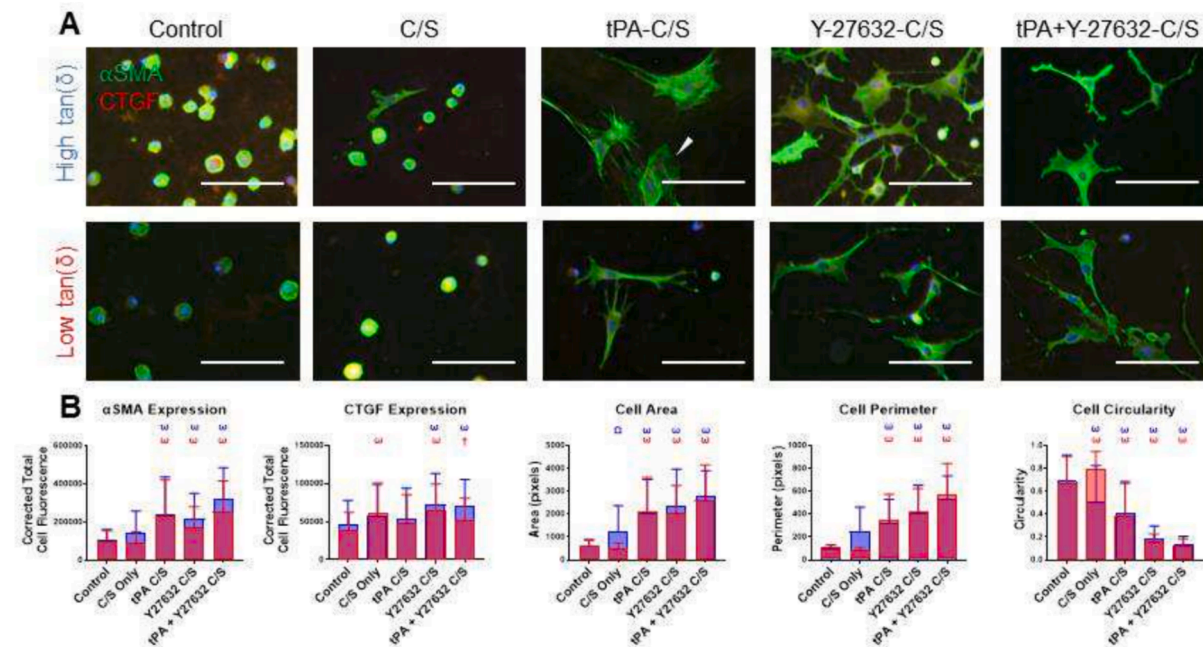


Fig. 5. Evaluation of neonatal rat cardiac fibroblasts comparing fibrotic markers and cell morphology on high and low loss tangent microgel thin films with drug-loaded nanogels. (A) Representative images of NRCF on high and low loss tangent microgel thin films. (B) Quantification of NRCF fibrotic markers on high (blue) and low (red) loss tangent microgel thin films with drug-loaded nanogel samples after 48 h. α SMA, CTGF, cell area, cell perimeter, and cell circularity measurements are shown. Stress fiber positive cells are indicated by white arrowheads. A one-way analysis of variance was conducted with a Tukey's post-hoc test using a 95 % confidence interval. Mean \pm standard deviation is shown. $\dagger p < 0.05$, $\ddagger p < 0.01$, $\Omega p < 0.001$, $\omega p < 0.0001$. Scale bar = 100 μ m. (For interpretation of the references to colour in this figure legend, the reader is referred to the web version of this article.)

(Fig. 9). Again, there was a morphological difference noted between HUVECs seeded on traditional and physiologically relevant *in vitro* platforms. On soft and stiff PA gels, HUVEC cell area and perimeter

decreased, and cell circularity significantly increased for cells treated with Y-27632 nanogels compared to controls. On high and low loss tangent films, there was an increase in cell area and perimeter, with a

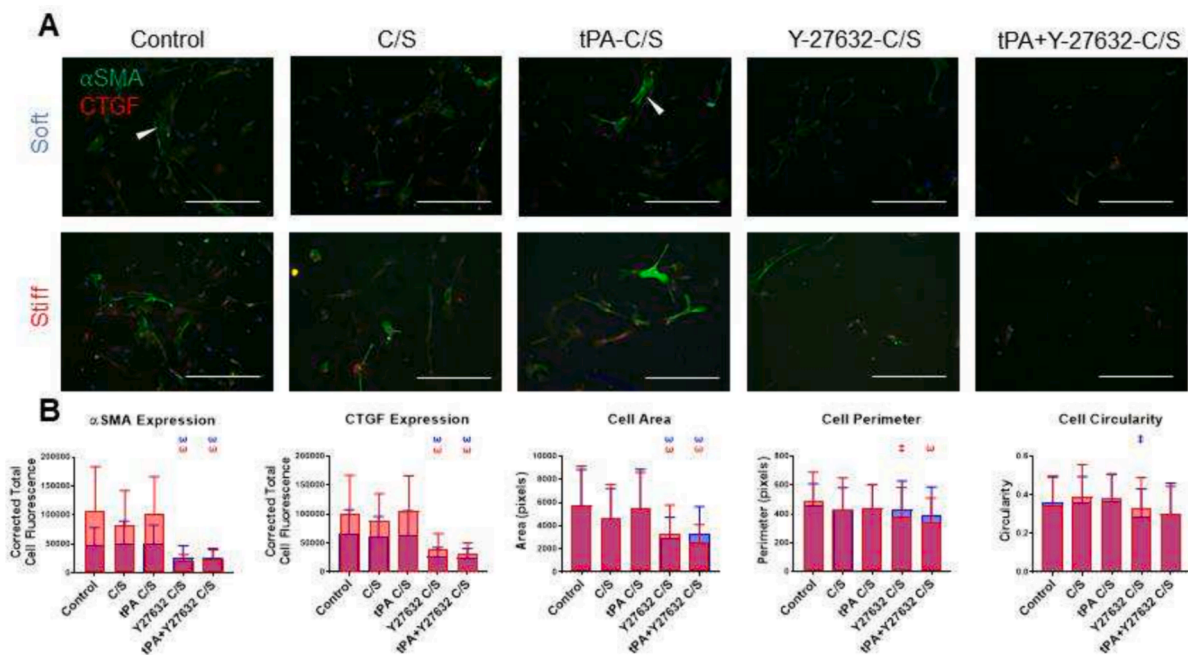


Fig. 6. Evaluation of human aortic smooth muscle cells (HASMC) comparing fibrotic markers and cell morphology on soft and stiff PA gels with drug-loaded nanogels. (A) Representative images of HASMC on soft and stiff PA gels. (B) Quantification of HASMC fibrotic markers on soft (blue) and stiff (red) PA gels with drug-loaded nanogel samples after 48 h. α SMA, CTGF, cell area, cell perimeter, and cell circularity measurements are shown. Stress fiber positive cells are indicated by white arrowheads. A one-way analysis of variance was conducted with a Tukey's post-hoc test using a 95 % confidence interval. $\dagger p < 0.05$, $\ddagger p < 0.01$, $\Omega p < 0.001$, $\omega p < 0.0001$. Scale bar = 400 μ m. (For interpretation of the references to colour in this figure legend, the reader is referred to the web version of this article.)

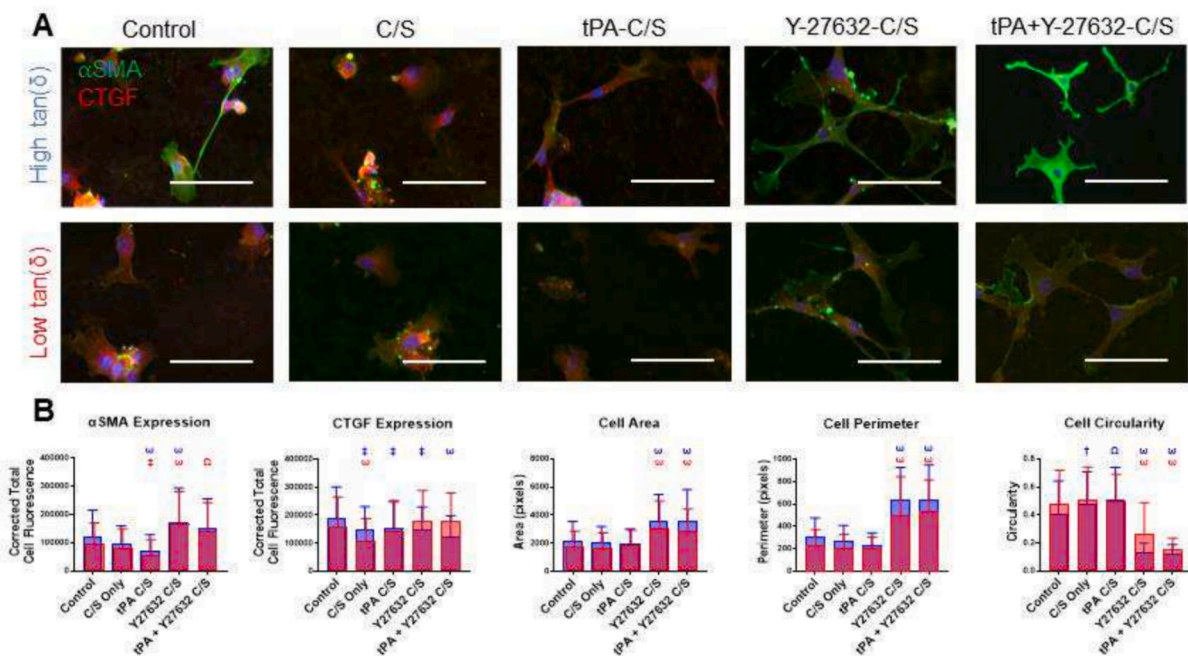


Fig. 7. Evaluation of human aortic smooth muscle cells (HASMC) comparing fibrotic markers and cell morphology on high and low loss tangent microgel thin films with drug-loaded nanogels. (A) Representative images of HASMC on high and low loss tangent microgel thin films. (B) Quantification of HASMC fibrotic markers on high (blue) and low (red) loss tangent microgel thin films with drug-loaded nanogel samples after 48 h. α SMA, CTGF, cell area, cell perimeter, and cell circularity measurements are shown. A one-way analysis of variance was conducted with a Tukey's post-hoc test using a 95 % confidence interval. $\dagger p < 0.05$, $\ddagger p < 0.01$, $\Omega p < 0.001$, $\omega p < 0.0001$. Scale bar = 100 μ m. (For interpretation of the references to colour in this figure legend, the reader is referred to the web version of this article.)

decrease in cell circularity, on controls samples compared to cells treated with Y-27632 nanogels. The models examined in this study demonstrate trends of antifibrotic drug delivery therapeutics will vary depending on the *in vitro* model used. Fibrotic response appears to be

mitigated on traditional PA gels, where therapeutic efficiency decreases on microgel thin films.

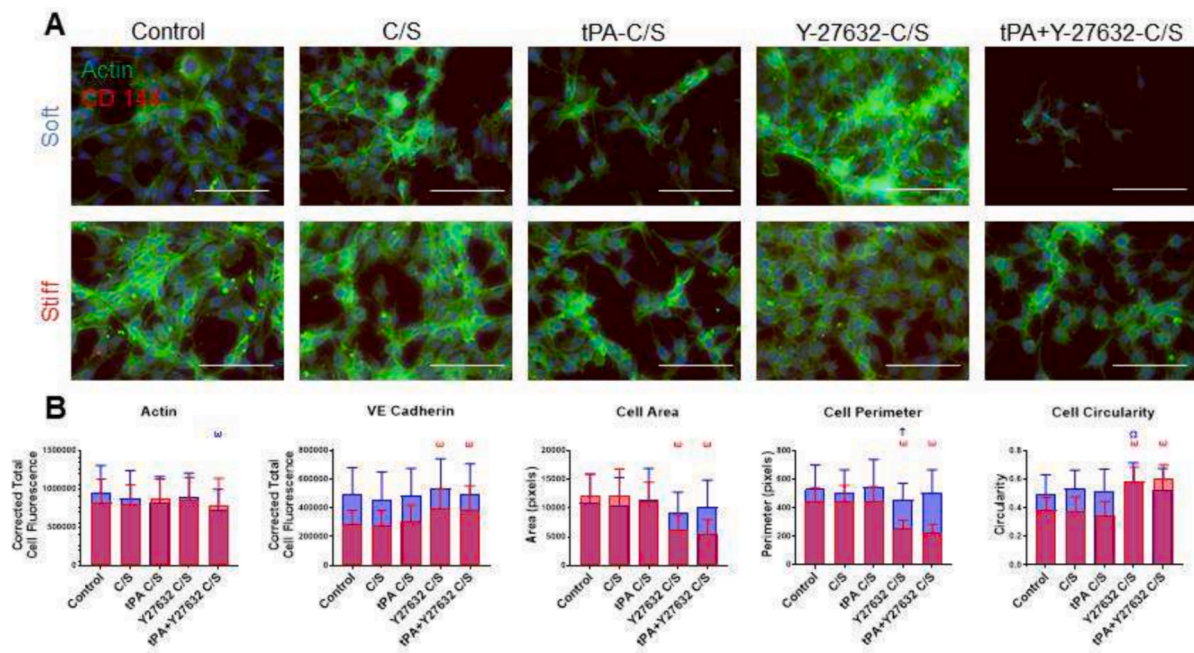


Fig. 8. Evaluation of human umbilical vein endothelial cells (HUVEC) comparing endothelial markers and cell morphology on soft and stiff PA gels with drug-loaded nanogels. (A) Representative images of HUVECs on soft and stiff PA gels. (B) Quantification of HASMC fibrotic markers on soft (blue) and stiff (red) PA gels with drug-loaded nanogel samples after 48 h. Phalloidin, VE Cadherin, cell area, cell perimeter, and cell circularity measurements are shown. A one-way analysis of variance was conducted with a Tukey’s post-hoc test using a 95 % confidence interval. Mean ± standard deviation is shown. †p < 0.05, ‡p < 0.01, Ωp < 0.001, ωp < 0.0001. Scale bar = 400 μm. (For interpretation of the references to colour in this figure legend, the reader is referred to the web version of this article.)

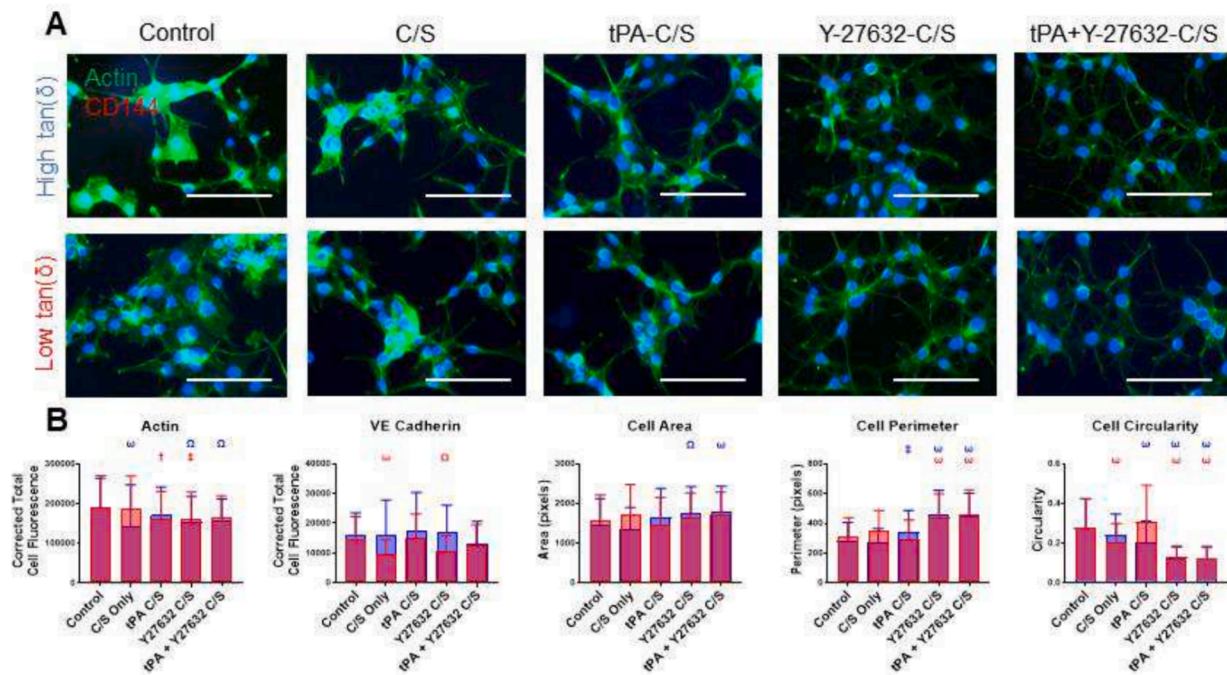


Fig. 9. Evaluation of human umbilical vein endothelial cells (HUVEC) comparing endothelial markers and cell morphology on high and low loss tangent microgel thin films with drug-loaded nanogels. (A) Representative images of HUVECs on high and low loss tangent microgel thin films. (B) Quantification of HUVECs fibrotic markers on high (blue) and low (red) loss tangent microgel thin films with drug-loaded nanogel samples after 48 h. Phalloidin, VE Cadherin, cell area, cell perimeter, and cell circularity measurements are shown. A one-way analysis of variance was conducted with a Tukey’s post-hoc test using a 95 % confidence interval. Mean ± standard deviation is shown. †p < 0.05, ‡p < 0.01, Ωp < 0.001, ωp < 0.0001. Scale bar = 100 μm. (For interpretation of the references to colour in this figure legend, the reader is referred to the web version of this article.)

tPA containing nanogels facilitate endogenous fibrinolysis

While the primary focus of these studies was to study anti-fibrotic

efficacy of dual-loaded nanogels, the fibrinolytic functionality of these particles is also a key component of this therapeutic for treating MI, therefore we also evaluated fibrinolysis of the particles. Endogenous

fibrinolysis was evaluated for C/S nanogels dual loaded nanogels with Y-27632 or tPA. Results from these studies (Supplementary Figure 2) demonstrated that C/S nanogels single loaded with tPA and C/S nanogels dual loaded with tPA + Y-27632 loaded nanogels demonstrate that tPA promotes clot degradation, as expected. In these studies, we also evaluated how loading plasmin into the nanogels, instead of tPA, influenced fibrinolytic capabilities. We found little evidence of degradation in the presence of lower concentrations (1 mg/mL) of nanogels single loaded with lower concentrations of plasmin or dual-loaded with plasmin and Y-27632. These results may be due to low concentrations of nanogels used and/or a low concentration of plasmin loaded into the nanogels. Increasing the plasmin concentration in loading solutions and increasing the nanogel concentration to 3 mg/mL in the fibrinolysis assay did lead to inhibition of clot polymerization, showing that plasmin could be used as an alternative to tPA in this dual loaded nanogel approach.

Evaluation of cell viability and nanogel endocytosis

We evaluated cell viability and potential nanogel endocytosis on soft and stiff PA gels. Cell viability was found to be 89 +/- 8 % and 71 +/- 17 % for HASMCs and 96 +/- 3 % and 82 +/- 17 % for HUVECs, on soft and stiff PA substrates, respectively. When cells were treated with dual-loaded nanogels, cell viability was found to be 87 +/- 13 %, 59 +/- 37 %, 91 +/- 8 %, and 84 +/- 18 %. We next evaluated the potential for nanogel endocytosis through confocal microscopy. Cells were incubated for 24 h with PBS of fluorescently labeled nanogels. Results showed evidence of endocytosis for both C/S nanogels and FSNs in all cell types on both soft and stiff substrates (Supplementary Figure 3). Fluorescent nanogels were observed within cells. Endocytosis of the nanogels could enhance drug delivery strategies when using these therapeutics in the future.

Discussion

In normal tissue repair and wound healing processes, regulated fibrosis is key to replacing the structural components of damaged tissue. Unfortunately, continued abnormal fibrosis leads to accumulation and deposition of ECM components, tissue scarring, and reduced tissue function. A common example of a progressive fibrotic disease is cardiac fibrosis, which occurs frequently after myocardial infarction. This enhanced scarring is mainly the role of differentiated cardiac fibroblasts (myofibroblasts), but other relevant cardiac cells will respond to changes in the chemical and mechanical microenvironment. Previous research has demonstrated actin stress fiber positive smooth muscle cells following exposure to platelet-derived growth factors (PDGF) [21]; a family of growth factors implicated in tissue fibrosis. Finally, research has also described the critical interactions of endothelial cells and smooth muscle cells for vascular homeostasis. In assessing the therapeutic efficacy of preventing cardiac fibrosis, we employed all three cardiac cell types (fibroblasts, smooth muscle, and endothelial cells).

A rat myocardium displays elastic modulus values of 10–20 kPa [22]. Additionally, nanoscale characterization of rat cardiac myocytes displayed a Young's Modulus of ~ 36 kPa [23]. With aging, or fibrotic diseases, an increased stiffness is anticipated due to cardiac ECM remodeling. In recapitulating the healthy and fibrotic cardiac microenvironment, this study utilized soft (~20 kPa) and stiff (~100 kPa) PA gels spanning this range. As a comparative analysis, to examine the influence of changes in viscosity during fibrosis on cellular response, viscoelasticity microgel thin films were also utilized. Currently the role of myocardial viscoelasticity is not well understood, but previous research has described changes in tissue viscoelasticity with increased fibrotic progression. Previous studies have noted a significant decrease in fibrotic liver (0.03) loss tangent values in comparison to healthy tissue (0.06) [24]. The loss tangent of the microgel thin films utilized for these studies were 1 % BIS (low): 1.8 +/- 0.1, 2 % BIS (medium): 1.5 +/- 0.1,

7 % BIS (high): 0.9 +/- 0.2. The film loss tangent implemented spans the magnitude difference noted between fibrotic and healthy tissue in previous studies.

These studies employ the use of two different viscoelastic substrates to mimic a range of ECM mechanics to examine the therapeutic efficacy of Y-27632 and tPA-loaded nanogels in various microenvironmental conditions. The cell types examined included NRFC, HASMC, and HUVECs cultured on soft and stiff PA gels compared to high and low loss tangent microgel thin films. A limitation of this study is only using immunofluorescence staining to evaluate cellular responses. The focus of this study was to gain a broad understanding of how different cardiac cell types respond to different mechanical environments by culturing cells on PA gels with varying Young's moduli and microgel thin films with varying loss tangents. We then evaluated how these different mechanical environments influence cellular responses to drugs. Due to the large number of conditions evaluated in these studies, we only used immunofluorescence staining to evaluate outcomes; however, future studies should also verify results by western blotting, quantitative PCR (qPCR), and functional assays such as fibroblast contraction. Our prior studies showed that α SMA expression, evaluated by qPCR [25], was influenced by both PA gel Young's moduli and microgel thin film loss tangent. Also, with decreasing loss tangent, an increase in fibroblast stiffness and contraction was noted [14]. Therefore, we expect these parameters to have a similar influence in the cell types utilized for these experiments.

The comparisons between responses on PA gels and microgel thin films allows for identification of how viscosity of the microenvironment influences cells responses to therapeutics. For the PA gel formulations used, the loss modulus values (G'') would be near 0 [26]. Previous studies have demonstrated the mostly elastic nature of PA gels [27]. Expressing loss tangent as the ratio of G''/G' (loss/storage modulus), with the loss modulus approaching 0, the loss tangent values for these PA gels would be near zero. However, with a similar elastic modulus for the fibrotic mimetics explored: 7 % microgel thin films and 100 kPa PA gels, we anticipate some result similarities. Our studies demonstrate a similar CTGF expression for NRFC, displaying a corrected fluorescence of 7 %: 118,907 +/- 76,654 (Fig. 1) and 100 kPa: 133,769 +/- 79,228 (Fig. 2). This trend is switched for HASMC, where CTGF expression is significantly higher on 100 kPa PA gels (Fig. 1). However, the α SMA expression is consistently higher on 7 % films in comparison to 100 kPa PA gels, for both HASMC and NRFC (Fig. 2). Again, these findings differ for HUVECs, where the Actin and VE Cadherin expression is significantly higher on 100 kPa PA gels (Fig. 1). Analyzing cell morphology results, for all cardiac cell lines explored, a significantly higher cell area and lower cell circularity was noted on stiff PA Gels (Fig. 1). This indicates that on 100kPa PA gels, the cells display more elongation which may provide insight into a myofibroblast phenotype.

While some similarities are noted between the 7 % 4-layer film and 100 kPa PA gel compared to less crosslinked films, they were not identical. Even the low loss tangent films have some degree of fluidity, highlighting that even small degrees of viscosity in the cellular environment can influence cellular responses. These nuances again highlight the importance of investigating cells in physiologically relevant environments, which employ the viscoelasticity of the microenvironment.

Conclusion

In previous studies administering tPA and Y-27632 nanogel carriers in an I/R injury rat model, significant reduction in infarct area and improved left ventricular ejection fraction (LVEF) was observed. However, Y-27632 administered alone was not sufficient to significantly reduce infarct size or fibrotic markers or improve LVEF 4 weeks post I/R injury, suggesting fibrinolysis may be a critical step in preventing fibrosis following MI and I/R injury¹⁶.

The results presented in this study highlight the importance of accurately representing healthy and fibrotic cardiac ECM mechanics.

Utilizing single loaded Y-27632 nanogels, reduced fibrotic markers on soft substrates and emerging fibrotic phenotypes on stiff PA gel substrates were noted in NRCF and HASMC. HUVECs did not show drastic changes in VE Cadherin expression on soft substrates, with a similar trend noted in Actin expression on stiff substrates. Additionally, on soft substrates there was not a significant change in cell morphology. Interestingly, treatment with single loaded Y-27632 nanogels encouraged fibrotic progression in NRCF and HASMC; noting an increase in α SMA and CTGF expression. However, differing results were observed when cells were cultured on physiologically relevant thin films. Specifically, HUVECs, on high loss tangent films, reduced actin and VE Cadherin expression with Y-27632 loaded nanogel treatment. On PA gels and microgel thin films, the development of actin stress fibers was noted in samples: 1) NRCF: Soft + Control, Soft + C/S, Soft + tPA-C/S, Stiff + Control, Stiff + C/S, and Stiff + tPA-C/S. 2) HASMC: Soft + Control, and Soft + tPA - C/S. 3) NRCF: High tan(δ) + tPA-C/S. These studies present an attractive therapeutic to mitigate fibrotic responses, using a Y-27632 ROCK inhibitor. Clinically, inhibition of Rho/ROCK pathway is not feasible. In previously published studies administering tPA and Y-27632 to treat ischemic and fibrotic related complications associated with MI, fibrin specificity was added to nanogel drug carriers to limit drug release to areas of fibrin rich thrombus and deposition.

Overall, we found that in the presence of Y-27632 containing nanogels, a reduction of fibrotic marker expression was noted on traditional healthy and fibrotic cardiac mimetics. These findings differed on physiologically relevant cardiac mimetics, where early treatment with the ROCK inhibitor intensified the fibrotic related responses. Because most natural ECMs are viscoelastic, these results demonstrate the importance of developing biomaterial systems that more closely match natural ECM mechanics to 1) better understand how ECM mechanics influence fibrosis related outcomes and 2) develop *in vitro* systems that more closely mimic *in vivo* ECM mechanics to evaluate therapeutic efficacy prior to *in vivo* studies. In conclusion, this work highlights novel developments in biomaterial design for mimicking ECM mechanics *in vitro* and investigating how ECM mechanics influence cellular responses and response to therapeutics.

CRediT authorship contribution statement

Aryssa Simpson: Writing – review & editing, Writing – original draft, Visualization, Validation, Methodology, Investigation, Formal analysis, Data curation, Conceptualization. **Emily P. Mihalko:** Writing – review & editing, Writing – original draft, Visualization, Methodology, Investigation, Formal analysis, Data curation, Conceptualization. **Caroline Fox:** Writing – review & editing, Methodology, Investigation, Formal analysis. **Smriti Sridharan:** Writing – review & editing, Methodology, Investigation, Formal analysis, Data curation. **Manasi Krishnakumar:** Writing – review & editing, Methodology, Investigation, Formal analysis, Data curation. **Ashley C. Brown:** Writing – review & editing, Writing – original draft, Visualization, Validation, Supervision, Resources, Project administration, Methodology, Investigation, Funding acquisition, Conceptualization.

Declaration of competing interest

The authors declare the following financial interests/personal relationships which may be considered as potential competing interests: Dr. Brown is a Co-Founder of Selsym Biotech, Inc., a start-up company

focused on hemostatic material design.

Data availability

Data will be made available on request.

Acknowledgments

The authors acknowledge the Cellular and Molecular Imaging Facility at North Carolina State University for assistance with confocal microscopy. This work was supported by grants from an American Heart Association Predoctoral Fellowship (18PRE33990338) (EPM), R01HL146701 (ACB), and Abram's Scholars funding (MK).

Appendix A. Supplementary data

Supplementary data to this article can be found online at <https://doi.org/10.1016/j.mbplus.2024.100150>.

References

- [1] D.J. Hausenloy, D.M. Yellon, *J Clin Invest* 123 (2013) 92.
- [2] V. Talman, H. Ruskoaho, *Cell Tissue Res* 365 (2016) 563.
- [3] P.-J. Wipff, D.B. Rifkin, J.-J. Meister, B. Hinz, *Journal of Cell Biology* 179 (2007) 1311.
- [4] B. Bhana, R.K. Iyer, W.L.K. Chen, R. Zhao, K.L. Sider, M. Likhitanpanichkul, C. A. Simmons, M. Radisic, *Biotechnology and Bioengineering* 105 (2010) 1148.
- [5] X. Huang, N. Yang, V.F. Fiore, T.H. Barker, Y. Sun, S.W. Morris, Q. Ding, V. J. Thannickal, Y. Zhou, *Am J Respir Cell Mol Biol* 47 (2012) 340.
- [6] R.G. Dean, L.C. Balding, R. Candido, W.C. Burns, Z. Cao, S.M. Twigg, L.M. Burrell, *J Histochem Cytochem* 53 (2005) 1245.
- [7] R.G. Wells, *Biochimica Et Biophysica Acta (BBA) - Molecular Basis of Disease* 1832 (2013) 884.
- [8] B. Hinz, *Proc Am Thorac Soc* 9 (2012) 137.
- [9] B. Hinz, *Nat Med* 19 (2013) 1567.
- [10] M.C. Markowski, A.C. Brown, T.H. Barker, *Journal of Biomedical Materials Research Part A* 100A (2012) 2119.
- [11] E. Mihalko, K. Huang, E. Sproul, K. Cheng, A.C. Brown, *ACS Nano* 12 (2018) 7826.
- [12] C.E. Kandow, P.C. Georges, P.A. Janney, K.A. Beningo, *Methods in Cell Biology*, Academic Press, 2007, pp. 29–46.
- [13] J. Zhu, *Biomaterials* 31 (2010) 4639.
- [14] D. Chester, R. Kathard, J. Nortey, K. Nellenbach, A.C. Brown, *Biomaterials* 185 (2018) 371.
- [15] J.R. Tse, A.J. Engler, *Current Protocols in Cell Biology* (2010) 47, <https://doi.org/10.1002/0471143030.cb1016s47>.
- [16] A.C. Vandergriff, M.T. Hensley, K. Cheng, *J vis Exp* (2015), <https://doi.org/10.3791/52726>.
- [17] E. P. Sproul, R. T. Hannan, A. C. Brown, in *Biomaterials for Tissue Engineering: Methods and Protocols* (Ed.: K. Chawla), Springer, New York, NY, 2018, pp. 85–99.
- [18] W. Wang, E.M. Lollis, F. Bordeleau, C.A. Reinhart-King, *The FASEB Journal* 33 (2019) 1199.
- [19] E. Dejana, F. Orsenigo, M.G. Lampugnani, *Journal of Cell Science* 121 (2008) 2115.
- [20] S. Jalali, M. Tafazzoli-Shadpour, N. Haghhighipour, R. Omidvar, F. Safshekan, *Cell Commun. Adhes.* 22 (2015) 79.
- [21] A. Pontén, E. Bergsten Folestad, K. Pietras, U. Eriksson, *Circulation Research* 97 (2005) 1036.
- [22] N. Amdursky, M.M. Mazo, M.R. Thomas, E.J. Humphrey, J.L. Puetzer, J.-P. St-Pierre, S.C. Skaalure, R.M. Richardson, C.M. Terracciano, M.M. Stevens, *Journal of Materials Chemistry B* 6 (2018) 5604.
- [23] S.C. Lieber, N. Aubry, J. Pain, G. Diaz, S.-J. Kim, S.F. Vatner, *American Journal of Physiology-Heart and Circulatory Physiology* 287 (2004) H645.
- [24] M. Yin, K.J. Glaser, A. Manduca, T. Mounajjed, H. Malhi, D.A. Simonetto, R. Wang, L. Yang, S.A. Mao, J.M. Glorioso, F.M. Elgilani, C.J. Ward, P.C. Harris, S.L. Nyberg, V.H. Shah, R.L. Ehman, *Radiology* 284 (2017) 694.
- [25] D. Chester, V. Lee, P. Wagner, M. Nordberg, M.B. Fisher, A.C. Brown, *Journal of Biomedical Materials Research Part A* 110 (2022) 1224.
- [26] Q. Wen, P.A. Janney, *Exp Cell Res* 319 (2013) 2481.
- [27] T. J. Petet, H. E. Deal, H. S. Zhao, A. Y. He, C. Tang, C. A. Lemmon, *RSC Adv* n.d., 11, 35910.